Electrochimica Acta 78 (2012) 32–39

Contents lists available at SciVerse ScienceDirect

Electrochimica Acta

journal homepage: www.elsevier.com/locate/electacta

Study of the electrochemical behavior of the "inactive" Li_2MnO_3

S. Francis Amalraj[a,*], Boris Markovsky[a,**], Daniel Sharon[a], Michael Talianker[b], Ella Zinigrad[a], Rachel Persky[a], Ortal Haik[a], Judith Grinblat[a], Jordan Lampert[c], Martin Schulz-Dobrick[c], Arnd Garsuch[c], Luba Burlaka[a], Doron Aurbach[a]

[a] Department of Chemistry, Bar-Ilan University, Ramat-Gan 52900, Israel
[b] Department of Materials Engineering, Ben-Gurion University of the Negev, Beer-Sheva 84105, Israel
[c] BASF SE, GCN/E, Ludwigshafen am Rhein, 67056, Germany

ARTICLE INFO

Article history:
Received 1 March 2012
Received in revised form 6 May 2012
Accepted 6 May 2012
Available online 18 June 2012

Keywords:
Li_2MnO_3 electrodes
Cycling
Structural analysis
Layered-to-spinel transition

ABSTRACT

In this work, we studied the cycling performance of initially inactive Li_2MnO_3 electrodes prepared from micron-sized particles, at 30 °C and 60 °C and possible structural transitions that this material can undergo due to de-lithiation. It was found that being activated at elevated temperatures, Li_2MnO_3 electrodes demonstrate a steady-state cycling behavior and reasonable capacity retention after aging at 60 °C. The main gases evolved during polarization of the Li_2MnO_3 electrodes are O_2 evolved from the structure and CO_2 and CO that can be formed due the reaction of oxygen with carbon black. It was found that a transformation of the Li_2MnO_3 layered structure into a spinel-like phase occurred during the initial charging of the Li_2MnO_3 electrodes, which were characterized as possessing domains of both layered and spinel-like structures. The results of the structural studies of these electrodes obtained by the X-ray diffraction and transmission electron microscopy were found to be in agreement with their Raman spectroscopic responses. We suggest that the mechanism of the charge compensation during the extraction of lithium at 60 °C involves both oxygen removal from the Li_2MnO_3 structure and the exchange between Li^+ and protons formed during the anodic oxidation of ethylene carbonate or dimethyl carbonate solvents in $LiPF_6$ solutions at high potentials (>4.5 V). It is assumed that the proton-containing structure $Li_{2-x}H_{x-y}MnO_{3-0.5y}$ is retained in a discharged state of the electrode and may decompose above 500 °C with the formation of Li_2O and manganese oxides accompanied by the release of water and CO_2.

1. Introduction

Lithiated manganese oxides like the spinel-structured $LiMn_2O_4$, $Li_4Mn_5O_{12}$, $Li_2Mn_4O_9$, $LiMn_{2-x}M_xO_4$, orthorhombic or monoclinic structured $LiMnO_2$, and other Li—Mn—O or Li—Mn—M—O compounds (M is one or more transition metal, *e.g.*, Co, Ni) are widely studied and can be used as positive electrodes in lithium batteries [1]. Lithium-rich, two-component integrated $xLi_2MnO_3{\cdot}(1-x)LiMO_2$ compounds with improved characteristics are the most promising cathode materials for advanced high-power and high-energy density lithium batteries for EV applications. This is due to the high capacities of $xLi_2MnO_3{\cdot}(1-x)LiMO_2$ compounds (>200 mAh/g) in comparison with conventional layered compounds such as $Li[MnNi]O_2$ or $Li[MnNiCo]O_2$ [2–5], but not on the account of stability and rate capability.

Although the Li_2MnO_3 monoclinic component of the integrated compounds is electrochemically inactive for lithium insertion and extraction between 2.0 V and 4.4 V, it has attracted the attention of several research groups [6–9]. Li_2MnO_3 with the tetravalent Mn-ion can be represented as $Li[Li_{1/3}Mn_{2/3}]O_2$ and has a similar layered structure to $LiMO_2$, possessing high potential of Li extraction (>4.5 V), and a high theoretical capacity of 460 mAh/g for total Li extraction. Consequently, Li_2MnO_3 can be considered as an interesting Li—Mn—O model compound. Chemically leached Li_2MnO_3 [10] or iron and ruthenium-substituted $Li_2Mn_{1-x}Ru(Fe)_xO_3$ materials were also studied [11,12]. The authors in Ref. [12] have shown, for instance, that $Li_2Mn_{0.4}Ru_{0.6}O_3$ electrodes demonstrated an improved electroconductivity and capacity around 170 mAh/g.

It was established by Delmas et al. [13] that Li_2MnO_3 possesses an O3-type structure where interslab octahedral sites are only occupied by Li^+-ions, while Li^+ and Mn^{4+}-ions (in a ratio of 1:2) occupy slab octahedral sites. The lithium ions in the Li-rich layered Li_2MnO_3 are mobile and can be extracted from the structure on charging. However, the mechanism differs from the conventional one (that includes the oxidation of a transition metal), since Mn^{4+} cannot be further oxidized to the Mn^{5+} valence state [6]. It is now

* Corresponding author. Tel.: +972 3 531 7665; fax: +972 3 738 4053.
** Corresponding author. Tel. +972 3 531 8832; fax. +972 3 738 4053.
E-mail addresses: sfaj1@yahoo.com (S. Francis Amalraj), markovb@mail.biu.ac.il (B. Markovsky).

0013-4686/$ – see front matter © 2012 Elsevier Ltd. All rights reserved.
http://dx.doi.org/10.1016/j.electacta.2012.05.144

accepted that charging Li_2MnO_3 electrodes results in Li^+ extraction accompanied by oxygen loss from the lattice. At elevated temperatures, the mechanism may involve an exchange of Li^+ with protons that can be formed by oxidation of alkyl carbonates (EC, DMC) in solution at high anodic potentials. However, the mechanism of the above electrochemical reactions with Li_2MnO_3 remains controversial [11].

Although several scientific reports on the electrochemical behavior of Li_2MnO_3 electrodes have already been published, it is important to study further their cycling performance at elevated temperatures, as well as possible phase transitions that this material can undergo. Therefore, the aim of the present work was to investigate how an "inactive" Li_2MnO_3 can be activated by charging the electrodes at 30 °C and 60 °C, to propose a possible mechanism for lithium extraction, and to follow the structural transitions that may occur due to de-lithiation, by X-ray diffractometry, high resolution electron microscopy and Raman spectroscopy. We also aimed at analyzing gas evolution during charging Li/Li_2MnO_3 cells and to suggest probable reactions that may occur with Li_2MnO_3 electrodes in EC-DMC/$LiPF_6$ solutions at potentials >4.5 V. The issues raised in this work should provide important insight re: understanding the behavior of the complex Li-rich, high capacity cathode materials which initially contain Li_2MnO_3.

2. Experimental

Li_2MnO_3 was prepared from Li_2CO_3 and $MnCO_3$ in a 1:1 ratio. The reactants were thoroughly mixed and calcined in alumina crucibles at 850 °C for 6 h in air. The calcined product was ground in a mortar and finally sieved through a sieve with mesh size 50 μm. For electrochemical measurements, two- and three-electrode cells in a 2325 coin-type configuration (parts purchased from NRC, Canada) were used with a Celgard, Inc. polypropylene separator. The working electrodes of the active mass around 4–5 mg were prepared from a mixture of Li_2MnO_3, carbon black and a polyvinylidendifluoride (PVdF) binder (8:1:1 by weight) on aluminum foil using the doctor Blade technique, as described in our previous reports [14]. A lithium disk and a lithium chip served as counter and reference electrodes. We also assembled pouch cells comprising bigger working electrodes (55–70 mg of the active material) with a geometric surface area of 15 cm^2. The construction of these cells enabled the extraction of a portion of the gaseous mixture formed during cycling for further analysis. Electrochemical cells were assembled in glove boxes filled with highly pure argon (VAC, Inc.). We used electrolyte solutions (high purity, Li battery grade) comprising dimethyl carbonate (DMC) and ethylene carbonate (EC) (weight ratio of 1:1) and 1 M $LiPF_6$ (Ube Industries, Japan, Li-battery grade, used as received). The content of hydrofluoric acid and water in this solution was not more than 30 ppm and 10 ppm, respectively. After assembling, the electrochemical cells were stored at room temperature for 12–24 h to ensure the complete impregnation of the electrodes and the separators with the electrolyte solution. The electrochemical measurements were carried out using a battery test unit, model 1470, coupled with a FRA model 1255 from Solartron, Inc. (driven by Corrware and ZPlot software from Scribner Associates, Inc.), and a multichannel battery tester from Maccor, Inc., Model 2000. Two-electrode cells were tested in the potential range of 2.0–4.6 V or 2.0–4.8 V using a constant current (CC) mode or a constant current–constant voltage (CC–CV) mode at various C-rates. All the potentials in this paper are given *vs.* Li/Li^+. The accuracy of the calculations of the electrodes' capacity in all the graphs presented herein is around 95%. The electrochemical measurements were performed at 30 °C and at 60 °C in thermostats. Raman spectra of the Li_2MnO_3 powder and electrodes were collected *ex situ* in a back-scattered configuration (a He–Ne laser at 632.8 nm) using a micro-Raman spectrometer LabRam HR 800 from Jobin-Yvon Horiba Inc. [15]. For electrodes, Raman spectra were measured from at least 5–7 different locations. X-ray powder diffraction (XRD) measurements were performed using an AXS D8 Advance diffractometer (Bragg-Brenatno focusing geometry $\theta/2\theta$, Cu Kα radiation, receiving slit 0.2 mm, scintillation counter, 40 mA, 40 kV) from Bruker, Inc. (Germany). The analysis of the XRD patterns was carried out with the PowderCell program [16], and the Fullprof [17] program was used for Rietveld analysis. TEM examinations of electrode materials were performed with a LaB_6-200 kV Jeol-2100 transmission electron microscope. Convergent beam electron diffractions (CBED) were taken using a 4 nm probe size. TEM samples were prepared by the methodology described by Gabrisch et al. [18]. The morphology of the Li_2MnO_3 particles was studied by a scanning electron microscope (Inspect^{TM} from FEI Company, USA) and their specific surface area was measured by the Brunauer, Emmett, and Teller (BET) method using a Gemini 2375, Micromeritics (multipoint mode). The particle size distribution was measured using a Mastersizer-2000. The chemical delithiation of Li_2MnO_3 was carried out by treatment in sulfuric acid (2 M solution) at 30 °C for 24 h and followed by washing the samples with the double distilled water. The gases evolved from the Li-cells during cycling were studied *ex situ* by a gas chromatography–mass spectrometry technique. For these studies, the gases were collected from pouch cells with a precision analytical gas syringe series A-2 (VICI Precision Sampling, Inc.) and transferred immediately to a GC–MS device. Thermogravimetry–mass spectrometry (TGA-MS) experiments were carried out using a TGA-Q500 device combined with a Pfeiffer Thermostar model mass spectrometer or Autospec Premier micromass technologies, under Ar atmosphere. The gas flow rate was 120 ml min^{-1}. We used alumina crucibles in the temperature range of 30–1000 °C with a heating rate of 10 °C min^{-1}. The amount of the sample loaded into the crucible was about 7 mg.

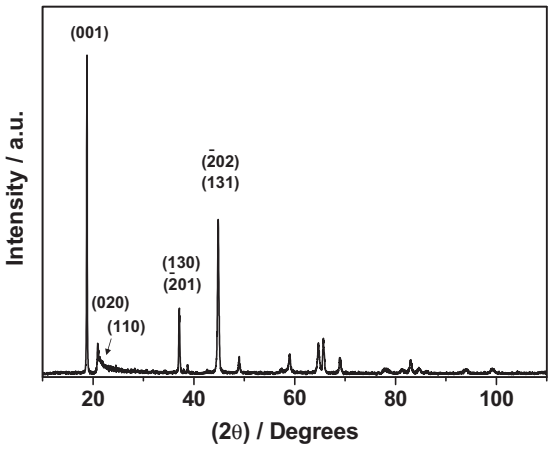

Fig. 1. XRD pattern of the pristine Li_2MnO_3 material. Miller indexes of main reflections are indicated.

3. Results and discussion

Fig. 1 presents the XRD pattern of the Li_2MnO_3 powder. The cell parameters obtained from the data by a standard least squares refinement procedure are as follows: $a = 4.9270(7)$ Å, $b = 8.5352(4)$ Å, $c = 5.0129(9)$ Å, $\beta = 108.91°$ (values $\alpha = \gamma = 90°$ were fixed). It is worth noting that the (0 2 0) and (1 1 0) peaks are substantially broad, thus merging into one broad peak located at the $2\theta° = 20$–22.5 range. As previously reported by other authors, this broadening can be attributed to the existence of structural defects such as faults in the stacking of the ordered cationic layers along the "c" monoclinic axis [19,13]. Microscopic measurements

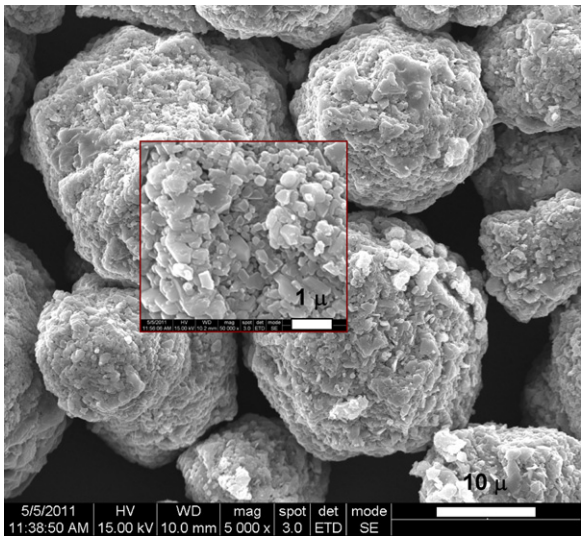

Fig. 2. SEM image of the Li_2MnO_3 particles.

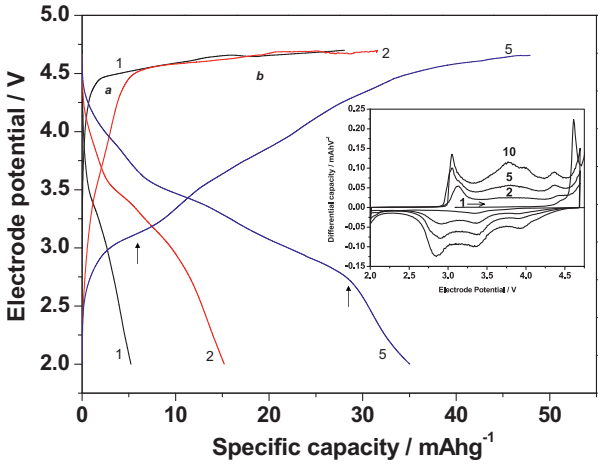

Fig. 3. Electrode potential *vs.* capacity plots measured at 30 °C during the 1st, 2nd, and 5th cycles in the potential range of 2.0–4.70 V from the Li_2MnO_3 electrode using the constant current mode. The current applied was 0.86 mA/g. Arrows indicate the electrochemical activity developed around 3 V. Coin-type cell, electrolyte solution used was EC-DMC (1:1)/$LiPF_6$. Insert: Differential capacity plots of the Li_2MnO_3 electrode measured at 30 °C. An intense irreversible peak above 4.6 V in the 1st charge relates to the oxygen evolution from the lattice. The numbers of cycles are indicated on the curves.

of the Li_2MnO_3 particles, Fig. 2, demonstrate that they are typically spherical micron-sized agglomerates comprising much smaller sub-micrometric irregular shaped particles. From a histogram of the particle-size distribution we concluded that it was represented by several fractions of the Li_2MnO_3 material, from 20 to 50 μm. The presence of particles of various sizes in this material, along with the existence of the structural stacking faults, may play a role in the electrochemical behavior of the "inactive" Li_2MnO_3 that is discussed below. The specific surface area of the Li_2MnO_3 powder used was around 0.86 m^2/g. Based on the literature reports on the electrochemical behavior of Li_2MnO_3 with micrometer particles and low specific surface area [9], it is expected that the material used in the present work should initially demonstrate poor electrochemical activity in Li-cells in term of specific capacity, especially at ambient temperature [9,20]. In turn, the relatively low surface area of Li_2MnO_3 used herein may be advantageous because of the high potential needed for its activation. At such a high potential, a high surface area active mass can catalyze detrimental oxidation reactions of the electrolyte solutions.

Fig. 3 presents typical potential *vs.* capacity profiles measured at 30° from these Li_2MnO_3 electrodes with the constant current of 0.86 mA/g in the potential range of 2.0–4.70 V. The voltage profile of the 1st charge demonstrates a rise (*a*) from OCV to 4.5 V, a plateau (*b*) above 4.5 V associated with Li-extraction and oxygen evolution from the host structure [23]. The first charge and discharge processes involve very low capacities, <30 mAh/g and around 5 mAh/g, respectively. However, it was established that upon repeated cycling between 4.7 and 2 V, the capacity increases, and the relative irreversible capacity decreases. Reversible lithium intercalation–deintercalation develops in the 2.5–4.5 V potential range. An electrochemical process is developed around 3 V during the cycling of these Li_2MnO_3 electrodes, as indicated with arrows at the charge and discharge profiles whose intensity increases with cycling. This electrochemical activity is evidently seen in the differential capacity plots of the Li_2MnO_3 electrodes at 30 °C demonstrated by the reversible anodic/cathodic peaks around 3 V and 4 V in the insert to Fig. 3, as well as it was found at 60 °C. As a first assumption, it is suggested that this electrochemical process reflects a phase transition associated with a partial layered-to-spinel transformation [21,22,24]. A similar behavior of the Li_2MnO_3 electrodes was also measured at 60 °C, as demonstrated in Fig. 4. This figure demonstrates the first and second voltage profiles of the Li_2MnO_3 electrode in constant current polarization up to 4.75 V. The current applied was 1.5 mA/g. The insert shows the differential capacity dQ/dE *vs.* potential curves, in which the reversible red-ox processes developed upon cycling can be clearly seen. It is evident that the first anodic processes of these electrodes lead to their gradual activation by a combination of de-lithiation and de-oxygenation. These activation processes form a Li_xMnO_y host of various stoichiometries, in which the Mn ions can change their oxidation state between 3^+ and 4^+, which enables reversible Li-ion intercalation.

Fig. 5 shows the typical cycling behavior (discharge capacity *vs.* cycle number) of the Li_2MnO_3 electrodes in the potential range of 2.0–4.65 V using the CC–CV mode (potentiostatic steps at 4.65 V for 3 h). The capacity increases upon repeated cycling at 60 °C and can reach 90–100 mAh/g. As it follows from this figure, dropping

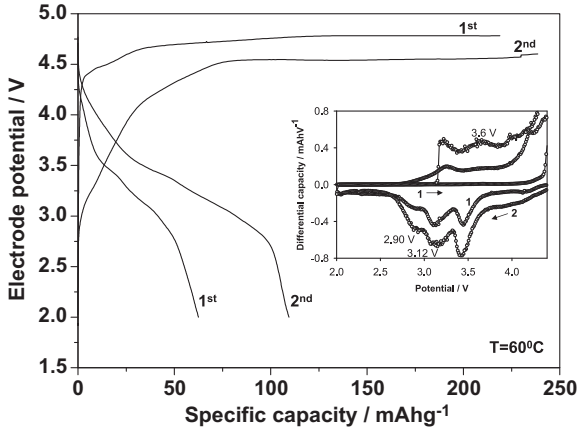

Fig. 4. Electrode potential *vs.* capacity plots measured at 60 °C during charge/discharge of a Li_2MnO_3 electrode. The current applied was 1.5 mA/g. This electrode underwent the 1st and 2nd charge/discharge cycles carried out in the potential ranges of 2.0–4.75 V and 2.0–4.60 V, respectively. After the 3rd charge to 4.60 V, this cell was disassembled and the electrode was studied by XRD, TEM (convergent electron micro-beam diffraction), and Raman spectroscopy. Insert: Differential capacity of the Li_2MnO_3 electrode measured at 60 °C. An intense irreversible peak of ~15 mAh/V at 4.50–4.55 V related to the oxygen evolution from the electrode is not shown in order to maintain an enlarged view of the cathodic and anodic waves/peaks of low intensity in the potential range of 3–4 V.

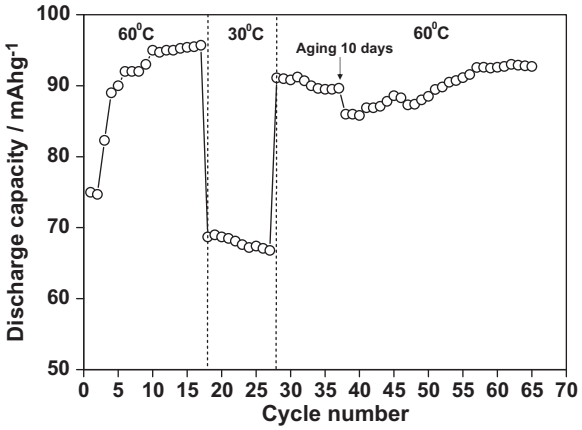

Fig. 5. Cycling and aging behaviors of the Li_2MnO_3 electrode in the potential range of 2.0–4.65 V. The current applied was 10 mA/g. The CC–CV mode was used with potentiostatic steps at 4.65 V for 3 h. The temperature of the cell was subsequently changed from 60 °C to 30 °C and finally to 60 °C; the cell was aged at the discharged state at 60 °C for 10 days, as indicated.

the temperature to 30 °C reduces the reversible capacity by 30%. The activation of Li_2MnO_3 electrodes at the elevated temperature and a subsequent cycling lead to a steady-state behaviors both at this temperature and after transferring the cell to 30 °C. It was also found that aging at 60 °C for 10 days did not influence much the discharge capacity.

Electrodes cycled at 60 °C were further measured by XRD and Raman spectroscopy. In Fig. 6, the XRD patterns measured from three Li_2MnO_3 electrodes activated at 60 °C are compared with the XRD profile of the pristine electrode. The electrode *a* was measured after the first charging by the CC–CV mode to 4.60 V at relatively high current, 1.5 mA/g. The charging capacity, and hence the level of activation, were relatively low, only 106 mAh/g (~25% of the theoretical capacity of Li_2MnO_3). The electrode *b* was charged first to 4.70 V followed by a potentiostatic step. The current applied was 1.5 mA/g and the total capacity obtained was 281 mAh/g (~61% of the lithium extracted). The electrode *c* (same as in Fig. 4) underwent the 1st and 2nd charge/discharge cycles carried out in the potential ranges of 2.0–4.75 V and 2.0–4.60 V, respectively, and charged finally to 4.60 V. The capacities delivered were 214, 230, and 274 mAh/g during the 1st, 2nd, and 3rd charge, respectively. The electrochemical cells containing electrodes *a*, *b*, and *c* were purposely terminated after the CC–CV charging and the 3rd charge,

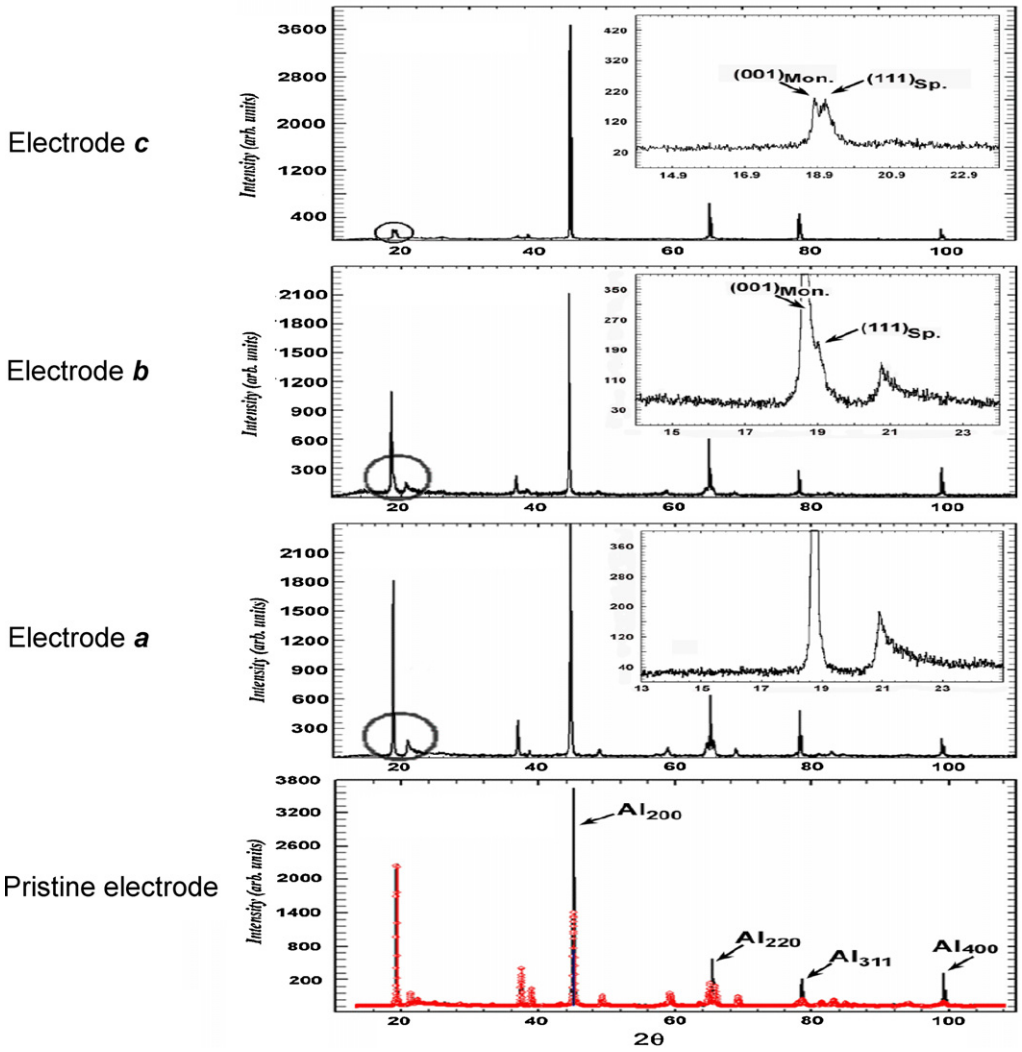

Fig. 6. XRD patterns recorded from the pristine Li_2MnO_3 electrode and from the de-lithiated Li_2MnO_3 electrodes, *a*, *b* and *c*, charged at 60 °C. The electrode *a* was charged first by the CC–CV mode to 4.70 V; the applied current was 1.5 mA/g. The electrode *b* was charged first to 4.70 V similarly to the electrode *a*. The electrode *c* (same as in Fig. 4) underwent the 1st and 2nd charge/discharge cycles carried out in the potential ranges of 2.0–4.75 V and 2.0–4.60 V, respectively, and charged finally to 4.60 V.

respectively and the electrodes were studied by XRD and Raman spectroscopy. Due to the fact that the Li_2MnO_3 electrodes were prepared on aluminum foil, all XRD patterns in Fig. 6 contain several strong peaks associated with aluminum. For clarity, the Al peaks are marked on the pattern presenting the pristine electrode. Also shown (in red) on this pattern is the calculated profile of the pristine Li_2MnO_3. As follows from Fig 6, there is no significant change in the XRD profile after the 1st charge of the Li_2MnO_3 electrode *a*. This observation correlates well with the relatively low value of the 1st charge capacity, 106 mAh/g. However, the diffractogram recorded from the electrode *b*, which delivered a much higher charge capacity, displays an additional very faint reflection appearing at $2\theta = 18.97^\circ$ (*d*-value = 4.671 Å) on the large-angle side of the (0 0 1) monoclinic peak. Substantial changes are also observed on the diffraction pattern taken from electrode *c*: the intensity of the strongest (0 0 1) monoclinic peak decreases dramatically, suggesting that the monoclinic structure is partially decomposed. Moreover, the peak associated with the monoclinic reflection (0 0 1) is split into two peaks, 4.724 Å and 4.668 Å that are clearly seen in the portion of the diffractogram on the enlarged scale. This implies that an additional phase is formed during charging. It was assumed that the 4.724 Å peak is related to the remaining monoclinic phase, while the 4.668 Å peak, as well as the faint 4.671 Å peak on the pattern obtained from electrode *b* can be interpreted as a (1 1 1) reflection of the $LiMn_2O_4$-type cubic-spinel structure. Based on this assumption, the Rietveld refinement method was employed to determine the unit cell dimensions of the spinel (*Fd-3m*) and monoclinic (*C2/m*) components. The following parameters were obtained: $a = 8.084(2)$ Å for spinel, and $a = 4.926(4)$ Å, $b = 8.557(4)$ Å, $c = 5.007(2)$ Å, $\beta = 109.35^\circ$ for the monoclinic phase. The decrease in the unit cell parameter of the spinel to the $a = 8.084(2)$ Å value in comparison with the value of 8.251 Å reported [25] for the spinel structure with the stoichiometric composition, $LiMn_2O_4$, may indicate a lithium deficiency in the spinel that is grown in the charged material. Another possibility is that the structure of spinel observed in the charged electrode is close to the family of proton-containing spinels and known as a cation-deficient spinel presented by a formula close to $Li_2Mn_4O_9$ with $a = 8.0916(2)$ Å [26].

Proof in support of the assertion that transformation from the layered structure to a spinel-like structure takes place during charging is also provided by electron microscopic observations. The electron micrograph in Fig. 7 presents an example of the particle observed in a specimen that was prepared from electrode *c* after the 3rd charge (same electrode of Figs. 4 and 6). The insert (*a*) in the micrograph shows a convergent beam electron diffraction pattern taken from the central part of the particle, in which the reflections are all indexed to a monoclinic unit cell of the Li_2MnO_3 phase with C2/*m* symmetry. However, it can be discerned that at the upper edge of the particle, in the region outlined by an ellipse, another particle has grown that exhibits a slightly different contrast. The corresponding CBED pattern shown in the insert (*b*) was indexed uniquely to the cubic spinel phase of the $LiMn_2O_4$ type. The results of the structural study of the Li_2MnO_3 electrodes *a*, *b*, and *c*, obtained by X-ray diffraction and TEM are in agreement with their Raman spectroscopic responses.

Fig. 8 compares the Raman spectra collected from the pristine Li_2MnO_3 electrode and from electrodes *a*, *b* and *c* (same as those related to Fig. 6). The Raman spectrum of the pristine electrode exhibits nine main well-resolved peaks located at 615, 569, 496, 438, 416, 372, 325, and 250 cm^{-1}, in agreement with the literature report [27] on the monoclinic Li_2MnO_3 phase. From the comparison of the Raman spectra obtained we conclude that the spectrum of electrode *a* charged once to 4.70 V at 60 °C, as well as of the spectrum measured from the Li_2MnO_3 electrode after the 1st charge to 4.70 V at a lower temperature, 30 °C (not shown here) are similar to the spectrum of the pristine electrode. These spectra show

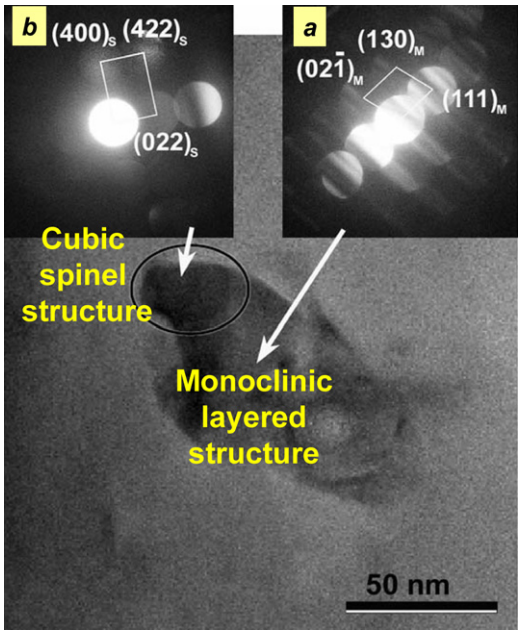

Fig. 7. TEM image obtained from the Li_2MnO_3 electrode *c* after the 3rd charge to 4.60 V. Voltage profiles of this electrode are represented in Fig. 4. Convergent microbeam electron diffraction patterns related to the monoclinic (M) layered and cubic spinel (S) structures of this electrode are shown in inserts *a* and *b*.

the same peak positions, but different peaks-intensity ratios (*e.g.*, at 615 cm^{-1} and 569 cm^{-1}) and demonstrate a broadening of these two peaks at 60 °C, as indicated in Fig. 8. The Raman responses from electrodes *b* and *c* (location 1) exhibit striking changes, namely a substantial decrease in the peaks' intensity, a blue shift of the main peak (attributed to the symmetric A_{1g} mode) to 640 cm^{-1} and its pronounced broadening, and a disappearance of a group of peaks located between 400 and 570 cm^{-1}. It can be suggested that the decreasing intensity and a blue shift are related to the lithium de-intercalation from the structure, increasing the electronic conductivity of the charged electrode [28] and to some cation mixing. The broadening of the Raman band may relate to a cationic disorder and to increasing the amount of stacking faults [29]. Similar phenomena were also observed in our previous study of the integrated $xLi_2MnO_3 \cdot (1-x)Li[MnNiCo]O_2$ electrodes cycled and charged to 4.80 V [15]. The disappearance of the Raman peaks at 400–600 cm^{-1} and a strong shift of the main band toward a high wavenumber of electrodes *b* and *c* in Fig. 8 can be ascribed to an irreversible manganese migration into the interlayer lithium sites that leads to the creation of a spinel-like cation ordering [30,31]. As follows from the literature reports, a strong Raman peak around 630 cm^{-1} is indeed associated with the cubic Li—Mn-spinel phase [32,33]. We have established that various locations (for instance, 1 and 2) of the Li_2MnO_3 electrodes *b* and *c* exhibited special Raman responses, as seen in Fig. 8. The Raman spectrum recorded from location 2 demonstrates a pronounced splitting of the main peak into two peaks positioned at 615 and 640 cm^{-1}, and a strong change in the peak at 569 cm^{-1}, while the rest of the Raman bands between 494 and 250 cm^{-1} remained almost unaffected. For instance, the ratios of peak intensities at 494 and 438 cm^{-1} are nearly the same: 1.44 for the pristine electrode and 1.50 for electrode *b*. These findings indicate that the charged Li_2MnO_3 electrode *b* can be characterized as possessing domains of both a layered structure and a cubic spinel-like structure (a characteristic peak at 640 cm^{-1}) as a result of the layered-to-spinel transition. The Raman spectral studies and the XRD measurements of the charged (activated) Li_2MnO_3 electrodes thus correlate quite well with those obtained from the

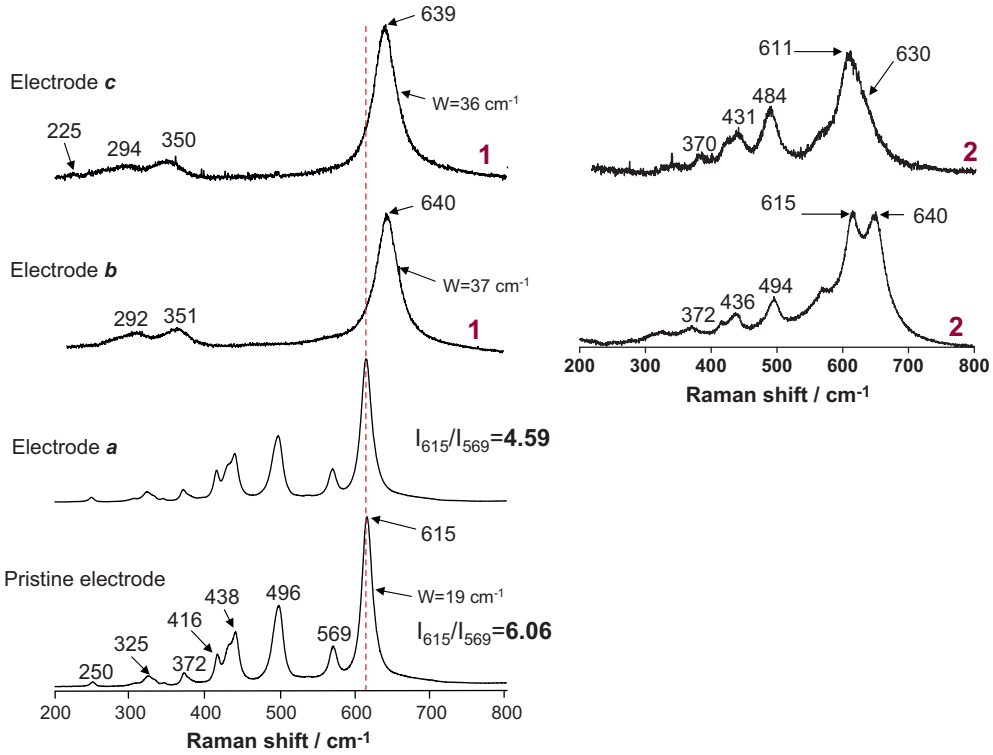

Fig. 8. Raman spectra measured from the pristine Li_2MnO_3 electrode and from the delithiated Li_2MnO_3 electrodes, *a*, *b*, and *c* charged at 60 °C (same electrodes as presented in Fig. 6). For electrodes *b* and *c*, the Raman spectra recorded from different locations, 1 and 2 are also shown.

Table 1
Relative amount of gases in the atmosphere of pouch cells measured by GC–MS. The pouch cells contained Li negative electrodes, composite Li_2MnO_3 or Al-foil positive electrodes and EC-DMC (1:1)/$LiPF_6$ solutions. The gases were detected after the 1st charge to 4.8 V of the Li_2MnO_3 electrode and during charging to 4.8 V of the aluminum electrode at 60 °C.

Moieties detected by MS	Relative amounts of gases	
	Li_2MnO_3 electrode	Aluminum electrode
CO_2	0.0650	0.0004
CO	0.0420	–
O_2	0.0120	–
H_2O	0.0065	0.0188
H_2	0.0050	–
HF	0.0045	–
$—C_2H_5$	0.0015	0.0024
$—CF_3$	0.0011	0.0004

electrochemical studies (electrode potential profiles, differential capacity plots) that also demonstrate the above transformation.

An additional and important piece of information was obtained in this work from the analysis (by GC–MS) of the gases evolved during the 1st charge of the Li_2MnO_3 electrodes at 60 °C in pouch cells. We also measured the atmosphere within similar pouch cells that contained Li anode, standard electrolyte solution and Al foil CC without active mass, stored at 60 °C. The data in Table 1 show that the main gases evolved in the 1st charge of the Li_2MnO_3 cathode at 60 °C are CO_2, CO, O_2, H_2 although the relative amount of oxygen is ~6 times lower than that of CO_2. These results agree quite well with the observations made by Yu et al. [9] at 60 °C. These authors also detected the above gases collected at 60 °C from a Li_2MnO_3 cell with an EC-based $LiPF_6$ solution in a similar quantitative order, namely, $CO_2 > CO > O_2 > H_2$. We suggest that CO_2 and CO can be formed due to the oxidative decomposition of EC or DMC accompanied by the development of protons, as described previously [34]:

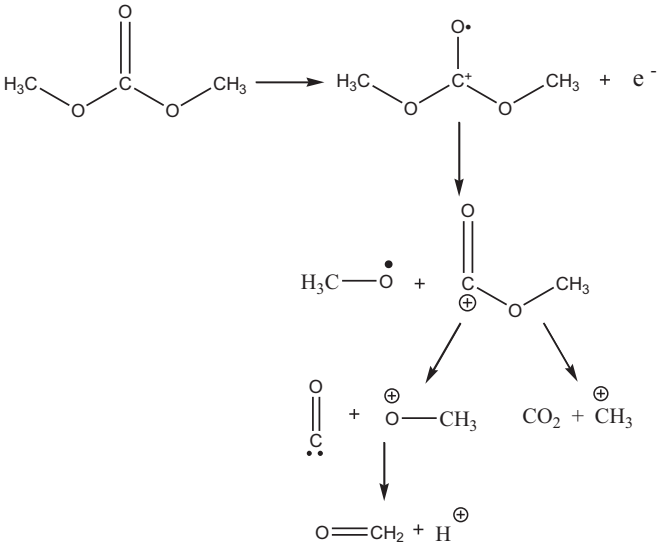

(1)

It is likely that a mechanism of the charge compensation during the extraction of lithium at 60 °C involves both oxygen removal from the Li_2MnO_3 structure and the exchange between Li^+ and H^+, as follows:

$$2O^{2-}(\text{lattice}) - 4e^- \rightarrow O_2(\text{gas}) \quad (2)$$

$$Li_2MnO_3 - ye^- + (x-y)H^+ \rightarrow Li_{2-x}H_{x-y}MnO_{3-0.5y} + xLi^+ + 0.25yO_2 \quad (3)$$

Removal of oxygen from the Li_2MnO_3 structure is evidently thermodynamically more favorable than the manganese oxidation to +5 state. The formation of $-C_2H_5$ and $-CH_3$ moieties can be explained by a partial decomposition of EC and DMC at high anodic potentials, or even by the decomposition of these solvent molecules during MS measurements. The oxygen evolved can react directly with the carbon black in the composite electrode to form CO and CO_2. Ethylene carbonate may react also with F^-, which acts as a nucleophile, and may form fluorinated organic moieties. Oxidation of the solution species (EC, DMC) at the Li_2MnO_3 electrode and corrosion of the aluminum foil current collector at high anodic potentials may also contribute to the overall charge capacity measured. As it follows from our voltammetric experiments at 60 °C, the anodic currents developed with Al electrodes in an EC-DMC/$LiPF_6$ solution at 4.3–4.8 V are around 0.47–0.68 μA/cm^2. Accordingly, the charge measured during the subsequent polarization of this Al electrode at 60 °C in the above potential range (each potentiostatic step for 4 h) is ~6.1 mC, only 0.098% of the total charge which is usually delivered by an Al/Li_2MnO_3 electrode, and therefore can be neglected. We have established that oxygen was not present in the gaseous mixture evolved during prolonged potentiostatic polarization of Al electrodes at high anodic potentials up to 4.8 V in an EC-DMC/$LiPF_6$ solution (Table 1). Consequently, we can conclude that oxygen is generated mainly from the Li_2MnO_3 cathode and is not a product of side reactions of the Al-current collector with solution species. Possible also is the following reaction between the HF unavoidably present in EC-DMC/$LiPF_6$ solutions and a Li_2CO_3 surface layer that is usually formed on the lithiated transition metal oxide particles [35]:

$$Li_2CO_3 + 2HF \rightarrow 2LiF + H_2O + CO_2 \quad (4)$$

The formation of protons included in the active mass after activation according to the above scheme (1) during the polarization of the Li_2MnO_3 electrodes at high anodic potentials was confirmed in this work by TGA-MS studies, as follows. The Li_2MnO_3 electrodes were cycled in the potential range of 2.0–4.7 V at 30 °C or 60 °C in pouch-cells. After disassembling the cells, rinsing the electrodes with DMC and drying under vacuum, TGA-MS tests were carried out as described previously [37]. In Fig. 9, we show the TGA and mass-spectra plots (*a* and *b*, respectively) of the following samples: pristine Li_2MnO_3 powder (1), chemically de-lithiated Li_2MnO_3 (2), charged Li_2MnO_3 electrode that provided the 1st charge capacity of ~51 mAh/g at 30 °C (3), Li_2MnO_3 electrode that delivered the 1st charge capacity of ~56 mAh/g and terminated at 2 V after 2 cycles at 60 °C (4), Li_2MnO_3 electrode (the 1st charge capacity was ~76 mAh/g) terminated at 4.7 V after 2 cycles at 60 °C (5), and of the mixture of PVdF + carbon black 1:1, by weight (6). It should be noted that the micro-sized Li_2MnO_3 particles used in this study are thermally stable. The pristine Li_2MnO_3 demonstrated a small weight loss (<2.5%, curve 1) in the TGA-MS experiment upon heating in argon up to 1000 °C. This is in agreement with the observation made by Strobel et al. [36] who established that millimeter-size crystals of Li_2MnO_3 are thermally stable up to at least 1100 °C (weight loss <0.5%). The thermal stability of the chemically delithiated sample (curve 2) decreases significantly and it decomposes above 140° C. The main decrease in the mass about 2.0% of this sample in the temperature interval of 140–240 °C is accompanied by release of H_2O (m/e = 18, Fig. 9b) and oxygen (m/e = 32) evolution similarly to the results in Ref. [38]. Hence, the content of protons in the chemically delithiated Li_2MnO_3 was calculated to be ~0.26. Taking into account the lithium content of 1.67 (calculated from the chemical analysis) and the Mn oxidation state of +4 (as estimated by XPS), the proposed bulk composition of the chemically delithiated sample can be written as $Li_{1.67}H_{0.26}MnO_{2.96}$. In regard of the main decrease in the mass of the charged Li_2MnO_3 electrode (curve 3), which is also accompanied with water release, it starts however at around

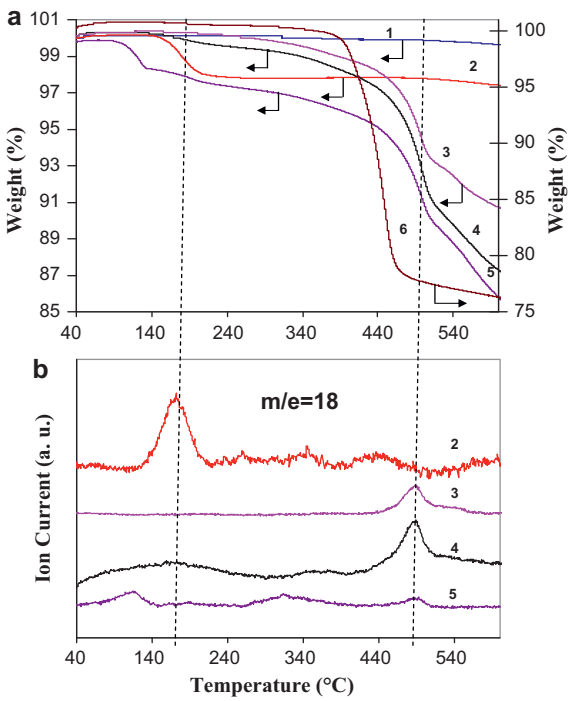

Fig. 9. Results of the TGA-MS experiments. Plot (*a*) shows the weight losses measured from: 1 – pristine Li_2MnO_3 material, 2 – chemically de-lithiated Li_2MnO_3 sample, 3 – charged Li_2MnO_3 electrode that provided the 1st charge capacity of ~51 mAh/g at 30 °C, 4 – Li_2MnO_3 electrode that delivered the 1st charge capacity of ~56 mAh/g and terminated at 2 V after 2 cycles at 60 °C, 5 – Li_2MnO_3 electrode (the 1st charge capacity was ~76 mAh/g) terminated at 4.7 V after 2 cycles at 60 °C, 6 – mixture of PVdF + carbon black (1:1, by weight). Plot (*b*) demonstrates mass spectrometry results for the water (m/e = 18) evolved from the chemically de-lithiated Li_2MnO_3 sample and from the cycled Li_2MnO_3 electrodes. Vertical dash lines are eye guides of the water evolution from the samples.

400 °C that is the onset temperature of the PVDF decomposition. This delay can be related to the porous structure of the electrode mass with a relatively high surface area of carbon black + PVDF that inhibits water desorption and oxygen release and, hence causes the holdup in the mass decreasing.

It is likely that the thermal decomposition reaction for the material of the charged/cycled electrode can be represented by the following scheme:

$$Li_{2-x}H_{x-y}MnO_{3-0.5y} \rightarrow (1-0.5x)Li_2O + (0.5x-0.5y)H_2O + MnO_2 \quad (5)$$

In order to subtract the weight loss related to decomposition of PVdF from the total weight loss (9.3%) of the electrode, reference experiments with a mixture of CB and PVdF 1:1, by weight (Fig. 9, curve 6) and with PVDF alone were carried out. By heating to 600 °C, PVdF losses of around 66% and the weight loss of the PVDF + CB mixture was 24% (not 33% as expected). Consequently, the weight loss of the PVDF + CB mixture subtracted from the total weight loss of the electrode should be 1/5th of 24%, namely 4.8%, since the electrode contained 20% of the PVdF + CB additives. The weight loss of the charged electrode in Fig. 9, curve 3 heated to 600 °C was, due to the Li_2MnO_3 decomposition alone, 4.5% (9.3% − 4.8% = 4.5%) accompanied with water and oxygen evolution. Finally, the true weight loss of the cycled Li_2MnO_3 electrode was 5.30%, from which the water content was calculated to be 2.36% (using the MS Lynxs software for the data treatment of the $H_2O + CO_2$ spectra). Consequently, the protonated phase $Li_{2-x}H_{x-y}MnO_{3-0.5y}$ contained ~0.31 protons. Based on the results represented in Fig. 9 we can conclude that the presence of water in the Li_2MnO_3 electrode material implies the formation of the proton-containing phase during

the anodic polarization and cycling of electrodes or by the chemical delithiation, in agreement with previously published reports [6,10,38,39].

4. Summary

In this work, we studied the electrochemical behavior of the "inactive" Li_2MnO_3 electrodes at 30 and 60 °C. It was established that typically at the initial charge, the electrode potential demonstrates a plateau above 4.5 V associated with Li-extraction and oxygen evolution from the host structure. We have found that the subsequent charging occurs at continuously lower potentials that can be associated with lower values of the chemical potential of the Li-ions in the cathode, indicating an activation of Li_2MnO_3 electrodes. These electrodes prepared from relatively large micron-sized particles can become active at 30 °C by applying low charge–discharge currents or by cycling at elevated temperatures. When activated at elevated temperatures, Li_2MnO_3 electrodes comprising micronic particles demonstrate a steady-state cycling behavior and reasonable capacity retention after aging at 60 °C. Using several analytical methods such as XRD, Raman spectroscopy, TEM, and the convergent micro-beam electron diffraction technique, it was found that a transformation of the layered structure into a spinel-like phase occurred during the initial charging of the Li_2MnO_3 electrodes. We also conclude from the above studies that the charged (activated) Li_2MnO_3 electrode can be characterized as possessing domains of both a layered structure and a cubic spinel-like structure due to the layered-to-spinel transition, correlating with the electrochemical results. We suggest that the presence of water in the Li_2MnO_3 cycled electrode material detected by the TGA-MS technique may relate to the formation of the proton-containing phase due to the Li^+ and H^+ ion-exchange during the anodic polarization of the electrodes at 60 °C or by the chemical de-lithiation of the pristine material in acid. By analyzing the gases evolved during the 1st charge of the Li_2MnO_3 electrodes at 60 °C, we have established that the main gases are carbon dioxide, carbon monoxide, oxygen, and hydrogen in the following quantitative order: $CO_2 > CO > O_2 > H_2$. The origin of CO_2 and CO may the oxidative decomposition of EC or DMC accompanied by the formation of protons (minor) and the reaction of the oxygen evolved during the course of Li_2MnO_3 activation with the carbon black (major). A comparison of the gases evolved from the Li_2MnO_3 cathodes and from the Al-electrodes polarized at high anodic potentials in EC-DMC/$LiPF_6$ solutions, leads to the conclusion that oxygen is generated mainly from the first cathode oxidation (and de-lithiation) and is not a product of side reactions due to oxidation of solution species. This is probably due to the well-developed passivation of the aluminum current collectors by their anodic polarization in $LiPF_6$-containing solutions. The $-CF_3$ moieties (minor) detected by the mass spectrometric measurements can be formed by reactions between fluorine radicals and the solvent molecules. Fluorine radicals may be formed by oxidation of F^- and PF_6^- upon the high anodic polarization applied to the solutions in the present study.

References

[1] J.-M. Tarascon, M. Armand, Nature (London) 414 (2001) 359.
[2] M.M. Thackeray, S.-H. Kang, C.S. Johnson, J.T. Vaughey, R. Benedek, S.A. Hackney, Journal of Materials Chemistry 17 (2007) 3112.
[3] J.-S. Kim, C.S. Johnson, M.M. Thackeray, Electrochemistry Communications 4 (2002) 205.
[4] J.-S. Kim, C.S. Johnson, J.T. Vaughey, M.M. Thackeray, S.A. Hackney, W. Yoon, C.P. Grey, Chemistry of Materials 16 (2004) 1996.
[5] C.S. Johnson, N. Li, C. Lefief, J.T. Vaughey, M.M. Thackeray, Chemistry of Materials 20 (2008) 6095.
[6] A.D. Robertson, P.G. Bruce, Chemistry of Materials 15 (2003) 1984.
[7] C. Gan, H. Zhan, X. Hu, Y. Zhou, Electrochemistry Communications 7 (2005) 1318.
[8] C.H. Lei, J.G. Wen, M. Sardela, J. Bareno, I. Petrov, S.-H. Kang, D.P. Abraham, Journal of Materials Science 44 (2009) 5579.
[9] D.Y.W. Yu, K. Yanagida, Y. Kato, H. Nakamura, Journal of the Electrochemical Society 156 (2009) A147.
[10] M.H. Rossouw, M.M. Thackeray, Materials Research Bulletin 26 (1991) 463.
[11] D. Mori, H. Sakaebe, M. Shikano, H. Kojitani, K. Tatsumi, Y. Inaguma, Journal of Power Sources 196 (2011) 6934.
[12] M. Tabuchi, Y. Nabeshima, K. Ado, M. Shikano, H. Kageyama, K. Tatsumi, Journal of Power Sources 174 (2007) 554.
[13] A. Boulineau, L. Croguennec, C. Delmas, F. Weill, Chemistry of Materials 21 (2009) 4216.
[14] Y. Talyosef, B. Markovsky, R. Lavi, D. Kovacheva, G. Salitra, M. Gorova, E. Zhecheva, R. Stoyanova, D. Aurbach, The Electrochemical Society Journals 154 (2007) A682.
[15] F. Amalraj, D. Kovacheva, M. Talianker, L. Zeiri, J. Grinblat, N. Leifer, G. Goobes, B. Markovsky, D. Aurbach, Journal of the Electrochemical Society 157 (2010) A1121.
[16] W. Kraus, G. Nolze, Journal of Applied Crystallography 29 (1996) 301.
[17] J. Rodriguez-Carvajal, Physica B 192 (1993) 55.
[18] H. Gabrisch, T. Yi, R. Yazami, Electrochemical and Solid-State Letters 11 (2008) A119.
[19] J. Breger, M. Jiang, N. Dupre, Y.S. Meng, Y. Shao-Horn, G. Ceder, C.P. Grey, Journal of Solid State Chemistry 178 (2005) 2575.
[20] G. Jain, J. Yang, M. Balasubramanian, J.J. Xu, Chemistry of Materials 17 (2005) 3850.
[21] C.S. Johnson, N. Li, J.T. Vaughey, M.M. Thackeray, Electrochemistry Communications 7 (2005) 528.
[22] S.H. Park, H.S. Ahn, G.J. Park, J. Kim, Y.S. Lee, Materials Chemistry and Physics 112 (2008) 696.
[23] H. Sommer, P. Lanz, M. Schulz-Dobrick, P. Novak, Paul Scherrer Institut, Annual Report, 2010, p. 46.
[24] C. Julien, Ionics 6 (2000) 30.
[25] H. Berg, J.O. Thomas, L. Wen, G.C. Farrington, Solid State Ionics 112 (1998) 165.
[26] A. Ibarra Palos, M. Anne, P. Strobel, Journal of Solid State Chemistry 160 (2001) 108.
[27] C.M. Julien, M. Massot, Materials Science and Engineering B100 (2003) 69.
[28] A. Abdel-Ghany, K. Zaghib, C.M. Julien, in: Z. Stoynov, D. Vladikova (Eds.), Portable and Emergency Energy Sources, Prof. Marin Drinov Publishing House, Sofia, 2006, p. 1.
[29] S. Nakashima, Y. Nakatake, H. Harima, M. Katsuno, N. Ohtani, Applied Physics Letters 77 (2000) 3612.
[30] R. Baddour-Hadjean, J.-P. Pereira-Ramos, Chemical Reviews 110 (2010) 1278.
[31] S.-J. Hwang, H.-S. Park, J.-H. Choy, G. Campet, J. Portier, C.-W. Kwon, J. Etourneau, Electrochemical and Solid-State Letters 4 (2001) A213.
[32] W. Huang, R. Trech, Journal of Power Sources 81–82 (1999) 616.
[33] H. Kanoh, W. Tang, K. Ooi, Electrochemical and Solid-State Letters 1 (1998) 17.
[34] M. Moshkovich, M. Cojocaru, H.E. Gottlieb, D. Aurbach, Journal of Electroanalytical Chemistry 497 (2001) 84.
[35] D. Aurbach, Journal of Power Sources 89 (2000) 89.
[36] P. Strobel, J.-P. Levy, J.-C. Joubert, Journal of Crystal Growth 66 (1984) 257.
[37] S.K. Martha, O. Haik, V. Borgel, E. Zinigrad, I. Exnar, T. Drezen, J.H. Miners, D. Aurbach, Journal of the Electrochemical Society 158 (2011) 1.
[38] J.K. Ngala, S. Alia, A. Dobley, V.M.B. Crisostomo, S.L. Suib, Chemistry of Materials 19 (2007) 229.
[39] Y. Paik, C.P. Grey, C.S. Johnson, J.-S. Kim, M.M. Thackeray, Chemistry of Materials 14 (2002) 5109.